J Bionic Eng 15 (2018) 805–819
DOI: https://doi.org/10.1007/s42235-018-0068-y

Journal of Bionic Engineering
http://www.springer.com/journal/42235

High Precision Data-driven Force Control of Compact Elastic Module for a Lower Extremity Augmentation Device

Likun Wang[1,2], Chaofeng Chen[1], Zhengyang Li[1], Wei Dong[1*], Zhijiang Du[1], Yi Shen[2], Guangyu Zhao[3]

1. *State Key Laboratory of Robotics and System*, *Harbin Institute of Technology*, *Harbin* 150001, *China*
2. *School of Astronautics*, *Harbin Institute of Technology*, *Harbin* 150001, *China*
3. *Weapon Equipment Research Institute*, *China Ordnance Industries Group*, *Beijing* 102202, *China*

Abstract

For human assistance device, the particular properties are usually focused on high precision, compliant interaction, large torque generation and compactness of the mechanical system. To realize the high performance of lower extremity augmentation device, in this paper, we introduce a novel control methodology for compact elastic module. Based on the previous work, the elastic module consists of two parts, *i.e*., the proximal interaction module and the distal control module. To improve the compactness of the exoskeleton, we only employ the distal control module to achieve both purposes of precision force control and human intention recognition with physical human-machine interaction. In addition, a novel control methodology, so-called high precision data-driven force control with disturbance observer is adopted in this paper. To assess our proposed control methodology, we compare our novel force control with several other control methodologies on the lower extremity augmentation single leg exoskeleton system. The experiment shows a satisfying result and promising application feasibility of the proposed control methodology.

Keywords: series elastic actuator, Human-Machine Interaction (HMI), force control, model prediction control, exoskeleton, bioinspired

1 Introduction

The past two decades have seen a renewed importance in the human assistance robot owing to its potential application in human strength augmentation[1–3], rehabilitation service[4–6] and interface of virtual reality[7,8]. Therefore, to reach the predestining target of the specified application, numerous studies have been devoted to designing novel control methodology and its mechanical structure.

Since the exoskeleton robotic system aims to follow to a specified task, i.e., stroke or rhythmic primitives, the sensor system should be able to provide the input signal to the controller. A typical design of the HMI proposed in the Hybrid Assistive Limb (HAL)[9] exoskeleton is focused on the Electro-Myo-Graphical (EMG) signals. Moreover, the intention is obtained from the pattern recognition technique. However, the main weakness of the above design is that the EMG signal heavily relies on the location of the sensors and the pattern recognition classifier is also different among different people.

An alternative is equipped with the sensor system according to the physical HMI, which is focused on the mapping from the physical interaction to incremental joint angle. Such interaction is usually derived from the impedance delivered from the exoskeleton to the user and vice versa[10,11]. Thus, the corresponding impedance controller is composed of an impedance dynamic model and a force controller[12,13]. For the application in Unluhisarcikli *et al*.[14] and Tsukahara *et al*.[15], the specified task is performed by the open-loop impedance controller without feedback from the force sensor. An improvement design is suggested by Carignan and Cleary[16]. In addition, the closed-loop position impedance controller is associated with the open-loop position control and feed forward term. Unfortunately, there is still considerable uncertainty with regard to model error.

To design compliant force control, the accuracy of the impedance dynamic model should be well considered, especially for a delicate haptic interface and rehabilitation therapy coping with the interaction

***Corresponding author:** Wei Dong
E-mail: dongwei@hit.edu.cn

force[17]. Consequently, several self-tuning methods of the impedance parameter are introduced by Bae and Tomizuka[18] to meet the corresponding demand. Moreover, a series elastic module has been proposed for the purpose of the requirement of high fidelity interaction force.

Although the interaction accuracy can be enhanced with the series elastic actuator, the unwilling interaction force owing to the uncertainty of the human-exoskeleton coupling model cannot be avoided[19]. Since the system identification of the dynamic model is not easy to obtain, a typical technique trick for dealing with the dynamic uncertainty is disturbance observer (DoB)[20]. Consequently, the uncertainty is compensated by the error between the observation from the DoB and feedback loop. However, a key problem with much of the literature is that such a controller highly depends on the accuracy of the prior knowledge of the control plant. Moreover, the stability and the performance of the corresponding control system also rely on the modeling precision.

To improve the performance of the control system in the presence of the time-delay and model uncertainties, a novel robust control methodology is suggested by Kim and Bae[21]. Disturbance and model uncertainties are canceled owing to the previous observation of the control input and system response. Such a feature is derived from the conception of the Time-Delay robust Control (TDC). In addition, since there is no need to identify the control system and gain scheduling, the desired performance can be maintained regarding the presence of the disturbance and model uncertainties. However, a strong assumption is that the system sampling frequency should cover the magnitude of the frequency of system uncertainties. Although the current technology of hardware might make the algorithm mentioned above possible, the improvement of the control system should not depend too much on the hardware.

Taking the above limitation into consideration, in this paper, the high precision data-driven force control system, a DoB is applied to mainly deal with the disturbance in terms of the human factors. For improvement of the closed-loop control performance, the model predictive control is utilized to handle constraints as well as model uncertainties.

Not akin to the work in Kong *et al*.[20], we aim to address the overall control issue as a discrete system, which is more straightforward in dynamic modeling and software programming. Moreover, the core idea of the control scheme[20] is the combination of the PD controller and the Linear Quadratic (LQ) method. Nevertheless, our main idea of the control scheme is based on the Model Predictive Control (MPC) theory. The main advantage of the MPC is the fact that it allows the current timeslot to be optimized, while keeping timeslots in account[42], thus differing from LQ. Also, the robustness is not only improved from the constraint of additive uncertainties but also from the internal model control theory.

The remainder of the paper is organized as follows, after the introduction, section **2** is devoted to discussing the mechanical designing of the compact elastic model in light of the biomechanical inspiration. In section **3**, the main routine of the control scheme is outlined, along with the discussion of the enhancement of the system robustness. The implementation of the experiments and the comparison of the control methods are presented in section **4**. Finally, section **5** concludes with a summary.

2 From the biomechanical inspiration

Concerning designing an exoskeleton, the biomechanics of human factors cannot be neglected, "since human legs have inherent damping as well as stiffness properties"[22]. In some daily life situations, the body does not act as an undamped spring and mass, *i.e*., standing up, sitting, walking and running. In addition, the viscous damping is of great significance in the functioning of human movement. From the other aspect, such a property plays a crucial role in stability maintaining as well as shock absorbing. However, much less attention has been paid to the designing from the biomechanical conception.

2.1 Pseudo-anthropomorphic

Generally, overall structural architecture is derived from the human biomechanics conception. Moreover, in light of mechanical designing analysis in Zoss *et al*.[23], to form a function exoskeleton, al-

most any designing layout falls into the following three types, *i.e*., anthropomorphic, Non-Anthropomorphic (NA) and Pseudo-Anthropomorphic (PA).

Anthropomorphic designing aims to match the human body properties exactly, such as joint range, limb length and misalignment. However, in practical, barely a perfect anthropomorphic architecture can achieve all the critical requirements ranged from joint misalignment to the exact end-effector matching. As an alternative designing conception, NA architecture is widely considered in many scenarios. As long as the pilot is not interfered by the robot, a wide range of possibilities can be implemented. Nevertheless, such a scheme is difficult to develop, since the foot is required for all the possible maneuvers (deep squats and turning tight corners). In addition, the collision between the pilot and the exoskeleton is a crucial issue owing to complicated development consideration. Thus, the safety concern brought by the collision should also be well addressed.

Considering the above limits, in this paper, the designing conception of our exoskeleton is based on the PA architecture. The PA is intended to choose a scenario which is nearly anthropomorphic. More specifically, the mechanical designing is almost kinematically similar to the human biomechanics. This means that the exoskeleton has three DoFs at both hip and ankle, while for knee joint only one DoF is designed in the sagittal plane. According to Clinical Gait Analysis (CGA), the range of exoskeleton should be larger than the range of human walking and less than the maximum range of human range of motion. Thus, our range of each joint is given in Table 1.

2.2 Elastic module prototype

Since the human joint owns features such as damping as well as stiffness, the Compact Elastic Module prototype (CEM) as shown in Fig. 1a is utilized to fulfill this requirement. From one aspect, the CEM is designed as a compliant torque generator, which transfers low impedance torque to actuate the exoskeleton torso. From the other aspect, the connection between the deformation of the CEM and its driven torque can be interpreted as an intrinsic force sensor. Thus, we seek to combine these two properties to achieve compliant force control.

Moreover, the control performance of the corresponding actuated joint mainly depends on the characteristics of such a CEM. If the CEM has a large stiffness, the pilot may feel uncomfortable. On the contrary, CEM should consider the above two facts, i.e., control performance as well as maximum torque.

In our previous work, a torsional spring has been designed to transfer the assistive torque, as shown in Fig. 1b. The torsional spring should be capable of high sensitivity to the HMI. Moreover, it should have the ability to prevent the control system from disturbance. The designed process is derived from the Finite Element Method (FEM). According to the iterative FEM analysis, the optimal structure has been selected as rotational symmetry. Note that, this kind of topological designing is superior to the symmetric structure[24].

We conduct a calibration experiment to obtain the static characterization of the CEM and the calibration platform is shown in Fig. 1c. The body of the CEM is fixed on the ground, while an encoder is mounted on the outer ring for deflection measurement. Additionally, the load torque is generated by the force-bearing bar. The test bed is connected to the bolt to keep stability. For signal collection, A Programmable Multi-Axis Controller (PMAC, Delta, USA) is applied to obtain the deflection of CEM by a magnetic encoder in real-time.

In the experiment, the maximum weight is 2 kg, while the minimum is 50 g. The test load cell ranges from 100 g to 2.5 kg with 50 g incrementally. In order to avoid the presence of noise disturbance, each value was tested for ten times. The results shown in Fig. 1d are chosen with 95% confidence. Moreover, it

Table 1 Joints ranges of motion

Joints	DoF	Scope (deg)
Hip	Flexion/extension	−30 – 90
	Adduction/abduction	−20 – 35
	Medial/extension	−35 – 35
Knee	Flexion/extension	0 – 85
Ankle	Plantarflexion/dorsiflexion	−30 – 25
	Pronation/external rotation	−25 – 15
	Inversion/eversion	−15 – 10

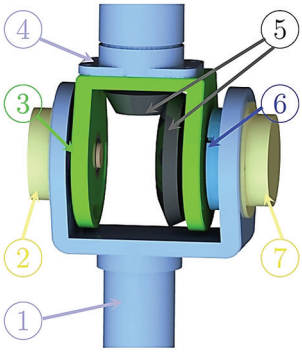

(a) Configuration of the compact elastic module

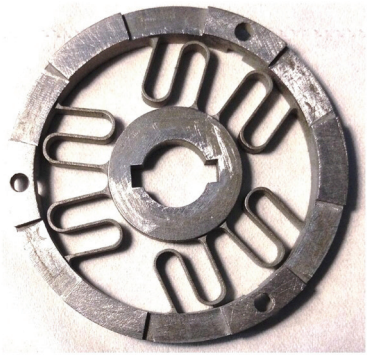

(b) The front view of the torsional elastic module

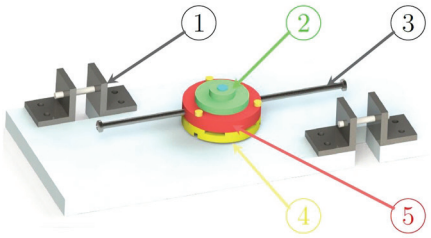

(c) The calibration platform

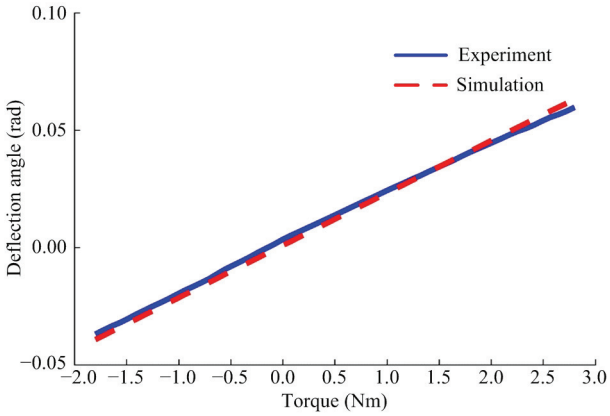

(d) Calibration result of the elastic module

Fig. 1 (a) As shown above, 1: the shank segment, 2: the encoder, 3: the encoder support, 4: the thigh segment, 5: bevel gear pair, 6: the torsional elastic module and 7: encoder; (b) the properties of the designed torsional elastic module are given in Table 2; (c) 1: bracket. 2: encoder, 3: force-bearing bar, 4: the torsional elastic module, 5: position pin; (d) the experimental data is presented in stat dots, while the simulation data are given in circle dots.

Table 2 Properties of the elastic module

Parameters	Values
Stiffness	60.2 Nm·rad^{-1}
Diameter of outer circle	60 mm
Diameter of inner circle	8 mm
Maximum torsion torque	4 Nm
Thickness	5 mm
Maximum deflection	0.087 rad

indicates that the stiffness is Ke = 60.2 Nm·rad^{-1}. Owing to the lack of space, for more information please refer to Long *et al.*[25].

2.3 Model representation

The assistive torque generated by the motor is transferred with the CEM. Therefore, the dynamics equation of the flexible joint is composed of two parts: *i.e.*, motor as well as HMI:

$$I_M\ddot{\theta}_M + C_M\dot{\theta}_M + k(\theta_M - \theta_H) = \tau_M, \quad (1)$$

$$I_H\ddot{\theta}_H + C_H\dot{\theta}_H - k(\theta_M - \theta_H) + mgl\sin(\theta_H) = \tau_H, \quad (2)$$

where the index M and H are defined as the motor and the human body segment respectively, I donates the inertia of the corresponding component, θ is the joint angle from neutral position, l is the distance between the center mass and the human joint center, m is the segment mass of human body, k is the elasticity coefficient obtained from the identification experiment, τ is defined as the joint torque.

For the convenience of analysis, we transform Eq. (2) into the normal viscous damping equation:

$$\ddot{\theta}_{\text{error}} + 2\lambda\dot{\theta}_{\text{error}} + \omega^2\theta_{\text{error}} = F_{\text{force}}, \quad (3)$$

where θ_{error} is the tracking error, λ is the damping coefficient, ω is defined as the systematic frequency and F_{force} is the forced term. Moreover, these terms are sat-

isfied with the following definition:

$$\theta_{\text{error}} = \theta_H - \theta_M, \tag{4}$$

$$2\lambda = \frac{C_H}{I_H}, \tag{5}$$

$$\omega^2 = \frac{k}{I_H}, \tag{6}$$

$$F_{\text{force}} = \frac{1}{I_H}(\tau_H - mgl\sin(\theta_H)). \tag{7}$$

According to the vibration theory[26], the ratio $\zeta = \lambda/\omega$ is introduced as the fraction of critical damping. If ζ is less than 1, the system is Under Damping; if ζ equals to 1, the system is Critical Damping; otherwise, the system is Over Damping. Considering the coefficients of damping and stiffness of human body joint in Granata *et al*.[27,28], the human dynamic system is Under Damping. From our tuition, the large damping coefficient results in too much dissipate energy. Therefore, naturally, the effective human joint movement requires not too much damping.

The designing conception of CEM aims to function human locomotion. Therefore, the constraints of above analysis should be also taken into consideration. From the point view of energy saving, Critical Damping will limit the feasibility application of exoskeleton in real daily life.

3 Control methodology for CEM

The input signal to the control system is obtained from the physical HMI, which is quantified by the deformation of the CEM. Thus, the controller should be capable of rejecting the undesired disturbance concerning the model uncertainties and measurement noise. In addition, the human factor may pose a threat to the control precision of the exoskeleton system.

The second crucial issue should be addressed is the time-delay effect caused by the physical HMI signal[29–31]. To achieve real-time control performance, the controller should be upgraded to the optimal parameters after every control closed-loop, i.e., forward loop and feedback loop. Moreover, the controller should be in a position to predict the next time-stamp control input on the purpose of decreasing the time-delay effect.

Therefore, the control scheme of the predictive force control is outlined in this section to meet the above demand of our exoskeleton system. In addition, to achieve precise control and safe physical HMI, the robustness of the proposed controller is carefully discussed from the point view of the internal model control[32,33].

3.1 Data-driven model predictive control

Data-driven control[43] aims to design the controller only relies on the input/output measurements data of the control plant as well as the sensor system, without explicitly or implicitly applying the dynamic information or whatever the model is linear or nonlinear. In this paper, the dynamic model is defined as an I/O discrete control plant and interpreted as a step response model. The overall control scheme is under the implementation of the Receding Horizon Optimization (data-stream optimization) and the Error Correction frameworks as detailed in this subsection.

The Newton's law and Hooke's law hold for:

$$\tau_{\text{HMI}} = \theta_{\text{error}} k. \tag{8}$$

The interaction torque measured from the CEM is defined as τ_{HMI}. From tuition, if the desired torque can be compensated by the joint motor, the desired position can be followed precisely. Thus, the desired position is defined as:

$$\theta_{\text{des}} = \theta_H + \frac{\tau_{\text{des}}}{k}. \tag{9}$$

Note that, the measured torque and the desired torque are not the same, since the presence of measured noise and friction cannot be avoided. According to Eq. (2), the transfer function from human joint angle θ_{H} to motor angle θ_{M} can be defined as:

$$\beta(s) = \frac{\Theta_{\text{error}}(s)}{\Theta_M(s)} = \frac{I_H s^2 + C_H s + mgl}{I_H s^2 + C_H s + k + mgl}, \tag{10}$$

where the term $\sin(\theta)$ in Eq. (10) is approximated as θ for analysis. Note that, I_{H} cannot be seen as the pure inertia of human leg segment since the physical HMI is not always the same. Moreover, in the single or double support phase of human locomotion, the inertia is increased dramatically owing to the contact with the ground. Therefore, $\beta(s)$ is a time-varying transfer function and depends on the physical HMI[20].

According to Eq. (8), the connection between the torque of rotary elastic spring as well as motor angle is given as:

$$\tau_{\mathrm{HMI}} = k(\phi\theta_M), \tag{11}$$

Therefore, we rewrite the Eq. (1) as:

$$I_M\ddot{\theta}_M + C_M\dot{\theta}_M + \tau_{\mathrm{HMI}} = \tau_M. \tag{12}$$

For simplification, the input of the model is assumed as $u(t) = \tau_M(t)$, while the output is given as $y(t) = \dot{\theta}_M(t)$. In addition, we transform the above Eq. (12) into the state space form:

$$\dot{y}(t) = \frac{1}{I_M}(u(t) - C_M y(t) - \tau_{\mathrm{HMI}}(t)), \tag{13}$$

Owing to $\dot{y}(t) = (y(t+1) - y(t))/T$ with sample period of T, the k step moment discrete-time predictive model is given as:

$$y(t+1) = (1 - \frac{T}{I_M}C_M)y(t) + \frac{T}{I_M}u(t) - \frac{T}{I_M}\tau_{\mathrm{HMI}}(t). \tag{14}$$

Since the partial derivatives of the next step output $y(t+1)$ respecting to the current output $y(t)$ and input $u(t)$ are continuous, the control system is generalized Lipschitz.

Predictive model: According to model predictive control theory[34,35], the plant model can be obtained by the step response model described in Eq. (14). Moreover, we assume that the output reaches the stability after sampling time N. Thus, the coefficients excited by the step response are defined as $a_1, a_2, \ldots, a_N$, where N is the length of the model time domain.

Based on the superposition principle of the control system, the system outputs are given by the contributions of the inputs

$$y_m(t) = \begin{cases} a_i\Delta\tau(t-i) & (1 \le i < N) \\ a_N\Delta\tau(t-i) & (i \ge N) \end{cases}, \tag{15}$$

Since only the past series inputs are known, we have to separate the sum into two parts, *i.e.*, before the current step and after the current step. Thus, the sum of a series of output predictions is described as:

$$\tilde{y}_m(t+i|t) = \tilde{y}_m^0(t+i|t) + \sum_{j=1}^{\min(M,i)} a_{i-j+1}\Delta\tau(t+j-1), i-1,\ldots,N. \tag{16}$$

A more compact description can be presented in a matrix form:

$$\tilde{\boldsymbol{Y}}_{\boldsymbol{m}} = \boldsymbol{A}\Delta\boldsymbol{\tau} + \tilde{\boldsymbol{Y}}_{\boldsymbol{m}}^0, \tag{17}$$

The matrices defined in Eq. (17) are given as:

$$\tilde{\boldsymbol{Y}}_m = [\tilde{y}(t+1|t), \tilde{y}(t+2|t), \ldots, \tilde{y}(t+n|t)]^{\mathrm{T}},$$
$$\Delta\boldsymbol{\tau} = [\Delta\tau(t), \Delta\tau(t+1), \ldots, \Delta\tau(t+M-1)]^{\mathrm{T}},$$
$$\tilde{\boldsymbol{Y}}_m^0 = [\tilde{y}_m^0(t+1|t), \tilde{y}_m^0(t+2|t), \ldots, \tilde{y}_m^0(t+P|t)]^{\mathrm{T}},$$

where M and P are the length of the control sequences and prediction sequences respectively ($M \le P \le N$). Additionally, the dynamic matrix $\boldsymbol{A}$, which is composed of the coefficients of the step response, shows the dynamic performance of the control system:

$$\boldsymbol{A} = \begin{bmatrix} a_1 & \cdots & 0 \\ \vdots & \ddots & \vdots \\ a_M & \cdots & a_1 \\ \vdots & \ddots & \vdots \\ a_P & \cdots & a_{P-M+1} \end{bmatrix}_{P\times M}.$$

Receding horizon optimization: For the purpose of improving the control performance, a possible solution is to find the 'best' control parameter vector $\Delta\boldsymbol{\tau}$ such that an error function between the desired trajectory and the actual trajectory is minimized. Therefore, the control object can be expressed through a 2-norm cost function:

$$J = \left\|\boldsymbol{y}_{\boldsymbol{m}}^d(t) - \tilde{\boldsymbol{Y}}_m(t)\right\|_Q^2 + \left\|\Delta\boldsymbol{\tau}(t)\right\|_R^2, \tag{18}$$

where $\boldsymbol{y}_{\boldsymbol{m}}^d(t)$ is the desired motor angle, while $\boldsymbol{Q}$ and $\boldsymbol{R}$ are the weighting parameters, with

$$\boldsymbol{y}_m^d(t) = [y_m^d(t), \ldots, y_m^d(t+P)]^{\mathrm{T}}, \tag{19}$$

$$\boldsymbol{Q} = \mathrm{diag}(q_1, \ldots, q_P), \tag{20}$$

$$\boldsymbol{R} = \mathrm{diag}(r_1, \ldots, r_M). \tag{21}$$

For a compact form, using Eq. (17) and necessary condition of minimum $\partial J / \partial\Delta\boldsymbol{\tau} = 0$, the optimal solution for control input is given as:

$$\Delta\boldsymbol{\tau} = (\boldsymbol{A}^{\mathrm{T}}\boldsymbol{Q}\boldsymbol{A} + \boldsymbol{R})^{-1}\boldsymbol{A}^{\mathrm{T}}\boldsymbol{Q}[\boldsymbol{y}_{\boldsymbol{m}}^d(t) - \boldsymbol{y}_{\boldsymbol{m}}^0(t)]. \tag{22}$$

Based on the receding horizon control principle, only the first sample of the sequence $\Delta\boldsymbol{\tau}$ is implemented, ignoring the rest part, thus:

$$\Delta\tau(t) = \boldsymbol{c}^{\mathrm{T}}\Delta\boldsymbol{\tau} = \boldsymbol{d}^{\mathrm{T}}[\boldsymbol{y}_m^d(t) - \boldsymbol{y}_m^0(t)], \tag{23}$$

with $\boldsymbol{c}^{\mathrm{T}} = [1, 0..., 0]$ and $\boldsymbol{d}^{\mathrm{T}} = (\boldsymbol{A}^{\mathrm{T}}\boldsymbol{Q}\boldsymbol{A} + \boldsymbol{R})^{-1}\boldsymbol{A}^{\mathrm{T}}\boldsymbol{Q}$.

Error correction: Due to uncertainties in dynamics and measurement noise, the precise prediction model is not easy to obtain. To improve the prediction of the incremental input, the error correction between the measured output and the predicted output is deployed to meet the demand

$$\tilde{\boldsymbol{y}}_m^{Cor}(t+1) = \hat{\boldsymbol{y}}_m(t) + \boldsymbol{h}e(t+1), \tag{24}$$

with $e(t+1) = y_m(t+1) - \hat{y}(t+1|t)$. Also, note that $\boldsymbol{h}=[h_1,\ldots,h_N]^{\mathrm{T}}$ is the weighting parameters of error correction. The term $\tilde{\boldsymbol{y}}_m^{Cor}(t+1)$ in Eq. (24) is the prediction sequences after error correction. The next step prediction can be obtained using one-step shift matrix

$$\tilde{\boldsymbol{y}}_m(t+1) = \boldsymbol{S}\tilde{\boldsymbol{y}}_m^{Cor}(t+1), \tag{25}$$

with the shift matrix defined as:

$$\boldsymbol{S} = \begin{bmatrix} 0 & 1 & & 0 \\ \vdots & \ddots & \ddots & \\ \vdots & & 0 & 1 \\ 0 & \cdots & 0 & 1 \end{bmatrix}. \tag{26}$$

Note that the error correction acts as the role of the state observer. Additionally, the performance of the control system is improved by the feedback control loop and the next step prediction is implemented on line by error correction.

3.2 Robustness improvement

Since the stability is crucial to the control system, the issue of performance robustness should also be addressed in terms of avoiding fine-tuning of gain scheming. This requirement is essential in the situation that the system dynamics vary significantly.

Considering our exoskeleton control system, the prediction model in Eq. (14) depends on $\beta(s)$ strongly, which varies in a large magnitude. Meanwhile, the source of disturbance mainly consists of dynamic uncertainties, human torque and systematic noise. In this paper, we apply disturbance observer (DoB)[36,37] for enhancing system robustness.

In terms of the disturbance, the set of control plant with the unstructured uncertainty of the human factors can be described as the perturbation $\Delta(z)$. Thus, the actual control plant is given as:

$$G_p(z) = z^{-m}G_n(z)(1+\Delta(z)), \tag{27}$$

where $G_n(z)$ is the nominal model. In addition, the time-delay term z^{-m} is identified by the system identification process.

Since the transfer function from the input $\tau(t)$, $d(t)$ and $\xi(t)$ to the output θ_m can be defined as:

$$G_\tau(z) = \frac{G_p(z)G_n(z)}{G_n(z) + [G_p(z) - G_n(z)z^{-m}]Q(z)}, \tag{28}$$

$$G_\xi(z) = \frac{G_p(z)Q(z)}{G_n(z) + (G_p(z) - G_n(z)z^{-m})Q(z)}, \tag{29}$$

$$G_d(z) = \frac{G_p(z)G_n(z)(1 - Q(z)z^{-m})}{G_n(z) + (G_p(z) - G_n(z)z^{-m})Q(z)}. \tag{30}$$

The close-loop characteristic is represented by the following polynomial function:

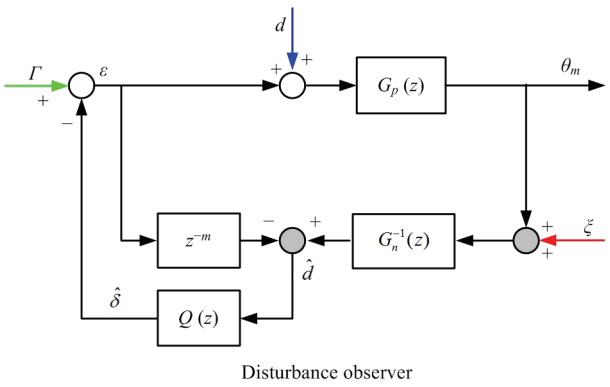

Fig. 2 The designing structure of discrete-time DoB. The DoB is used to estimate the disturbance and to compensate for the systematic uncertainties. For our control scheme, the DoB is mainly applied to deal with the interaction disturbance the pilot and the exoskeleton.

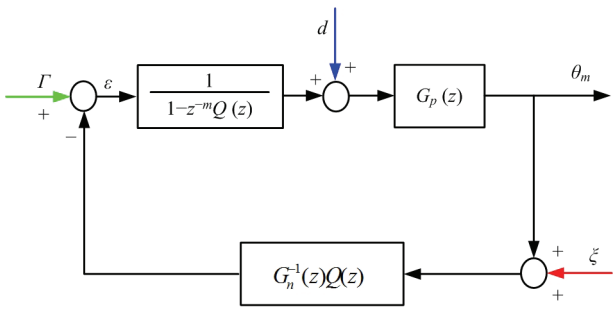

Fig. 3 Reformulated form of the DoB for analysis purpose corresponding to Fig. 2.

$$A_c(z) = G_n(z) + [G_p(z) - G_n(z)z^{-m}]Q(z), \quad (31)$$

Substituting Eq. (27) into Eq. (31), we obtain:

$$A_c(z) = G_n(z)(1 + z^{-m}\Delta(z)Q(z)). \quad (32)$$

Based on the robust stability[38], the sufficient and necessary conditions for DoB to be stable are that the zeros of transfer function are all fall into the unit circle, thus:

$$|z^{-m}\Delta(z)Q(z))|\Big|_{z=e^{j\omega}} < 1, \forall\omega. \quad (33)$$

According to the above analysis, in order to maintain the stability of the control system, the design of the filter $Q(z)$ is crucial such that the following constraint should be noticed:

$$|Q(z)| < |z^{-m}\Delta(z)|^{-1}\Big|_{z=e^{j\omega}}, \quad (34)$$

For the dependence of $Q(z)$ on $\Delta(z)$, the priority task is to design the perturbation $\Delta(z)$. As mentioned before, in the situation of single support and double support, the inertia of the human leg is dramatically increased[39]. Thus, the transfer function has an extremum, reaching to zero. This situation can be well explained that if the pilot has a steady pose with double support, the exoskeleton is supposed to maintain the same joint position. Due to the difference between the two cases, the perturbation can be designed as:

$$\Delta(z) = e^{-T_d s}\frac{(1-\beta(s)k)}{I_M s^2 + C_M s + \beta(s)k + C(s)}\Big|_{s=\frac{z-1}{T}}. \quad (35)$$

In light of Eqs. (28), (29) and (30), the output θ_M is given as:

$$\theta(t) = G_\tau(z)\tau(t) + G_d(z)d(t) + G_\xi(z)\xi(t), \quad (36)$$

where G_τ, G_d and G_ξ define the transfer function from motor torque, human factors and measurement disturbance, separately. In the low-frequency range, where the filter $Q(z) \approx 1$ the undesired human disturbance is eliminated with $G_d \approx 0$ and the system dynamics behave as the nominal plant $G_n(z)$. In this situation, the low-frequency disturbance has been observed with $G_\xi \approx 1$, and also the robustness is well guaranteed.

On the contrary, in the high-frequency domain, the filter $Q(z) \approx 0$, the DoB is not sensitive to the measurement noise due to $G_\xi = 0$. Additionally, the human torque is considered in the perturbation term $\Delta(z)$ which is compensated in the feedback loop.

3.3 Internal model properties

The Internal Model Control (IMC) aims to provide a straightforward design method, which is based on the perfect control structure theoretically. Additionally, the IMC has several fundamental properties, such as Dual Stability Criterion, Perfect Controller and Zero Offset.

Property I: Dual stability criterion: If the control model is perfect, the whole system stability depends on the sufficient condition of the stability of plant as well as the controller.

Property II: Perfect controller: If the control model is perfect and invertible, thus, the perfect tracking control can be achieved, although there exist disturbances.

Property III: Zero offset: The controller yields no offset, if the following condition is satisfied, *i.e.*, $G_z(1) = G_m^{-1}(1)$ and $G_F(1) = 1$.

For the convenience of analysis, we transform the DMC control block into IMC structure. According to Eqs. (15), (24) and (25), the corresponding prediction of time step k+1 can be written as:

$$\boldsymbol{\theta}_m(t+1) = \boldsymbol{S}[\boldsymbol{\theta}_m(t) + \boldsymbol{a}\Delta\tau(t) + \boldsymbol{h}e(t+1)]. \quad (37)$$

Based on the *z-transform*, a compact form can be obtained as:

$$\boldsymbol{\theta}_m(z) = \boldsymbol{l}_{\Delta\boldsymbol{u}}\Delta\tau(z) + \boldsymbol{l}_e(ze(z)), \quad (38)$$

with $\boldsymbol{l}_{\Delta\boldsymbol{u}} = (z\boldsymbol{I} - \boldsymbol{S})^{-1}\boldsymbol{S}\boldsymbol{a}$ and $\boldsymbol{l}_e = (z\boldsymbol{I} - \boldsymbol{S})^{-1}\boldsymbol{S}\boldsymbol{a}$.

Then, applying *z-transform* to the definition of $e_m(t+1)$:

$$\begin{aligned} ze(z) &= z\theta_m(t) - z\hat{\theta}_m(z) \\ &= z\theta_m(t) - \boldsymbol{c}^{\mathrm{T}}[\tilde{\boldsymbol{\theta}}_{\boldsymbol{m}}(z) + \boldsymbol{a}\Delta\tau(z)] \\ &= z\theta_m(t) - \boldsymbol{F}_{\Delta\tau}\Delta\tau(z) - \boldsymbol{F}_e(ze(z)), \end{aligned} \quad (39)$$

where $\boldsymbol{c}^{\mathrm{T}} = [1, 0, ..., 0]$, $\boldsymbol{F}_{\Delta\tau} = \boldsymbol{c}^{\mathrm{T}}\boldsymbol{l}_{\Delta\tau} + \boldsymbol{c}^{\mathrm{T}}\boldsymbol{a}$ and $\boldsymbol{F}_e = \boldsymbol{c}^{\mathrm{T}}\boldsymbol{l}_e$.

In order to obtain the internal-model form, the Eq. (39) further can be presented as:

$$e(z) = \theta_m(t) - z^{-1}\boldsymbol{F}_{\Delta\tau}\Delta\tau(z) - \boldsymbol{F}_e e(z). \quad (40)$$

Therefore, we obtain control block in Fig. 4.

Introducing $\varepsilon(z) = \theta_m(t) - z^{-1}\boldsymbol{F}_{\Delta\tau}\Delta\tau(z)$ and

$d_s = \sum_{i=1}^{P} d_i$, we have:

$$e(z) = \frac{\varepsilon(z)}{(1 + \boldsymbol{F}_e)}. \tag{41}$$

The equivalent transformation is shown in Fig. 5, meanwhile we obtain the IMC structure in Fig. 6. Additionally, the equivalent model, controller and filter are listed hereafter:

$$G_m(z) = \frac{z-1}{z} z^{-1} \boldsymbol{F}_{\Delta\tau}, \tag{42}$$

$$G_c(z) = \frac{z}{z-1} \frac{d_s}{1 + \boldsymbol{b}^{\mathrm{T}} \boldsymbol{G} \boldsymbol{l}_{\Delta\tau}}, \tag{43}$$

$$G_F(z) = \frac{\boldsymbol{d}^{\mathrm{T}} \boldsymbol{G} \boldsymbol{l}_e z}{d_s} \frac{1}{F_e}. \tag{44}$$

For further analysis, if the pilot keeps a static pose, the reference input should also keep as a constant input sequence $\boldsymbol{\theta}_m^d(t) = [\theta_m^d(t), ..., \theta_m^d(t)]^{\mathrm{T}}$; if there is a difference between human joint and motor angle, the desired input is defined as $\boldsymbol{\theta}_m^d(t) = [\theta_m^d(t+1), ..., \theta_m^d(t+P)]^{\mathrm{T}}$, which can be seen as human joint tracking control task.

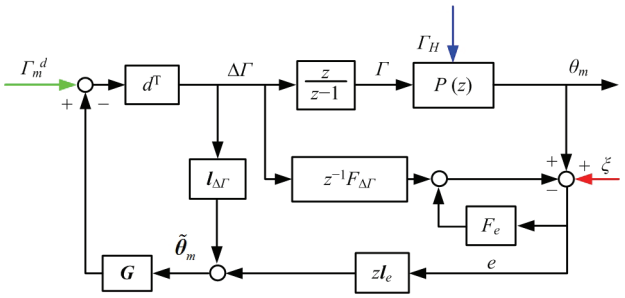

Fig. 4 The control scheme diagram. Note that the control plant is described in Fig. 3. The control pant is composed of the nominal plant and the DoB compensation.

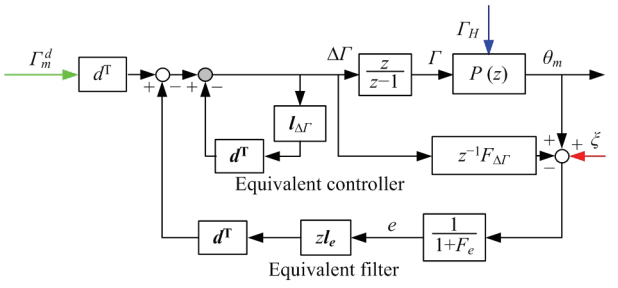

Fig. 5 The reformulated IMC form of the force control diagram corresponding to Fig. 4. The force control scheme has been transformed into the IMC structure. We demonstrate that our proposed control methodology owns the fundamental properties of the IMC. These properties can enhance the robustness and performance of our exoskeleton control system.

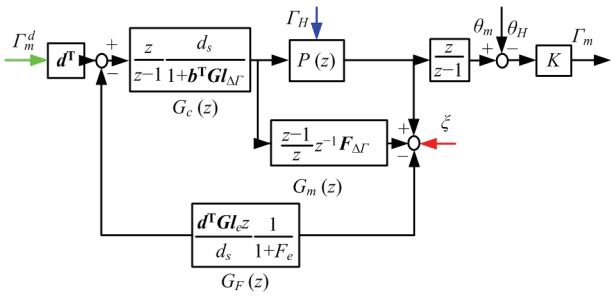

Fig. 6 The whole control scheme. For simplification, the proposed control has been transformed into the internal model control scheme, the controller $G_c(z)$ set the control signal to both the nominal plant $P(z)$ and the forward model $G_m(z)$. If the forward model is perfect, there will be no difference between the outputs from the two control plants. Otherwise, the difference will be compensated according to the feedback control loop. The filter $G_F(z)$ can be seen as a lower pass filter and maintain the stability of the control system.

In terms of the control stability, the system requires dual stability criterion, i.e., the stability of control plant as well as the controller. The robustness of the control plant is not difficult to obtain since the stability is guaranteed by the DoB and the uncertainty cancellation by the filter. If the length of the control steps P is large enough, despite any form of the step response $\{a_i\}$, the stability of the controller can be guaranteed. Nevertheless, in extreme situation $P \to \infty$, the control scheme is defined as mean level control, which the controller can only maintain a stable control but cannot change the dynamic performance of the system.

The zero offset derived from the designing of the filter $G_F(z)$. According to Eqs. (39) and (44) can be re-written as:

$$G_F(z) = \frac{\omega(z)}{d_s h(z)}, \tag{45}$$

with $\omega(z) = \sum_{i=1}^{N} (\omega_i - \omega_{i-1}) z^{-i}$, $c_i = \sum_{j=1}^{P} d_j h_{i+j-1}$ and $h(z) = \sum_{i=2}^{N} = 1 + (h_i - h_{i-1}) z^{-(i-1)}$.

For the feasibility of the designing of the filter $G_F(z)$, the weighting parameters h_i are chosen as:

$$h_1 = 1, h_i = \alpha, i = 2, ..., N, 0 < \alpha < 1, \tag{46}$$

It means that the prediction for the next time step is

uniformly corrected by weighting parameter α. Thus, we have

$$\begin{cases} h(z) = 1 + (\alpha - 1)z^{-1} \\ c(z) = \alpha d_s \end{cases}. \tag{47}$$

In addition, the filter is equivalent to a first-order filter

$$G_F(z) = \frac{\alpha}{1 - (1-\alpha)z^{-1}}. \tag{48}$$

Note that, as α in the range of $(0,1]$, the filter $G_F(z)$ is stable and the steady-state gain is given as $G_F(z)$=1. Moreover, according to Xi[40], it can also prove that the rest requirement of the zeros offset can also be met.

Thus, the control scheme is summarized below,

(1) First, the desired position of the motor is obtained from the spring deflection in real-time. If there is no difference between the position of the motor and the human joint angle, the exoskeleton will maintain a resting state.

(2) Second, the input to the control plant consists of the signal from the inner loop of the DoB compensation and the signal from the outer loop according to the receding horizon optimization and error correction. Note that, the outer loop control input is designed in terms of the nominal control plant (exoskeleton dynamics).

(3) Third, the unstructured disturbance mainly consists of the human interaction and the model uncertainties. Thus, to reject the variation of the model uncertainties and compensate for the human factors, the DoB is employed to enhance the control performance. In addition, the outer loop robustness can be analysed from the point view of the internal model control.

(4) Finally, if the outer loop controller is perfect, also the DoB can compensate the human interaction and reject for all the high-frequency disturbance, the control plant can follow the desired position precisely. Otherwise, the controller will optimise the control parameters and add the tracking error to the next time-step input.

4 From the biomechanical inspiration

In this section, to improve the robustness of the control system, the Q filter is designed according to the requirement for the DoB. In order to assess the control performance of the proposed control scheme, we test it with the other two control methods, *i.e.*, PID and PID with Smith predictor. In addition, a double actuated experiment is implemented on the single-leg exoskeleton platform to verify the validity of our proposed control methodology.

4.1 Q filter designing

Choosing the Q filter for the DoB is a crucial task of the entire control scheme. The Q filter is applied to guarantee robust stability. In designing, the magnitude of the filter should be in the boundary of the multiplicative uncertainties.

The main issue we have to address is that the Q filter is to keep the balance between the disturbance rejection as well as the robustness against the measurement noise. However, the designing process is quite intuitive since the properties of the observed loop are taken into consideration. Generally, the main purpose of the DoB aims to limit the disturbance at low frequencies and compensate the uncertainties in order to match the nominal plant. The candidate form of Q filter is given as:

$$Q(s) = \frac{\sum_{j=0}^{M} (\tau s)^j}{(\tau s + 1)^N}, \tag{49}$$

where the above is a third order (M=3) standard filter equation, while the time constant τ is given as 0.15, 0.075 and 0.03, as shown in Fig. 7. To choose the optimal time constant τ, the constraints in Eqs. (33) and (34)

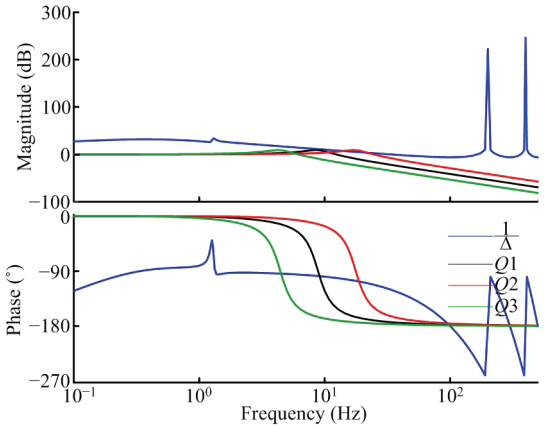

Fig. 7 Designing of the Q filter. The three candidates of the Q filter are indicated above. According to the designing conception, the Q filter should remain below and closed to uncertainties 1/Δ. Also should note that, the magnitude of the Q filter should cover the bandwidth of the human locomotion.

should be satisfied, which means that the magnitude response of Q filter should remain below and closed to $1/\Delta$. Thus, it is obvious that the time constant should be defined as 0.15.

4.2 Frequency response analysis

To improve the control performance, the designed compact elastic actuator should be able to track the desired input over large sufficient frequency range. It means that the inertia of the control plant is effectively eliminated and the system dynamics are well controlled by the actuator.

Thus, for generating precision desired torque, the frequency range of controller with the CEM should cover the frequency range of human locomotion 4 Hz – 8 Hz[39]. As shown in Fig. 8, the proposed controller can cover the frequency of 10 Hz, which can be seen as a satisfying design according to the experiment results above.

4.3 Control scheme evaluation

The experiment was conducted on a single leg exoskeleton platform. This platform is an ergonomic and robust device for strength augmentation purpose. The necessary auxiliary facilities for control enclosure are PMAC, embedded PC, Copley actuators and power supply unit. Considering our situation, the power module should produce three kinds of voltage, *i.e*., 5 V, 12 V and 24 V. The actual position signal is collected by PMAC, while the high-level control algorithm is calculated in the embedded PC. The driven commands are sent to the actuator through the Copley driver. For human intention recognition, the deformation of elastic torsional springs is detected by the magnetic encoders.

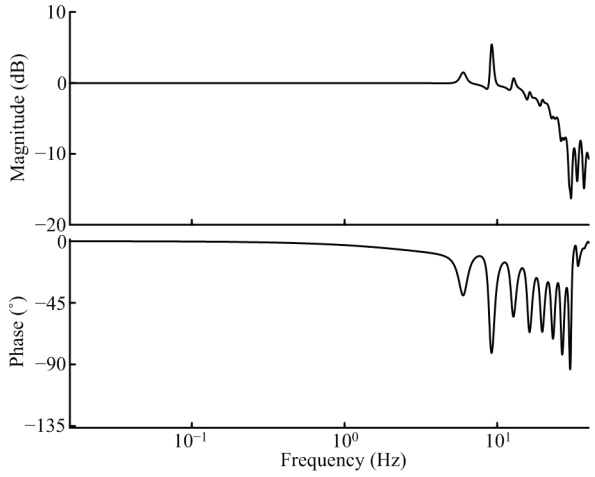

Fig. 8 Frequency response of our proposed control scheme. The basic property of the controller is that it should have enough magnitude of frequency in response to the human locomotion.

Safety consideration is a key issue since the human is closely in contact with the exoskeleton. Thus, we guarantee our pilot safety from hardware precaution as well as software precaution. Exceeding the range of human movement is avoided by the mechanical limits. In addition, both the hip joint and the knee joint are designed with an upper and lower boundary. The real-time current is detected by the control software, and the control system will shut the current down unless the current is in the setting range.

The first experiment is single joint tracking, which was performed to check the control performance of the proposed methodology without the human factor. In this experiment, we compare our proposed control scheme with a PID controller and a PID controller with the Smith predictor. For three control schemes, the input signal is all the same sinusoidal function.

With CEM, the actuator owns low impedance properties. This can be seen as an advantage in the interaction between the robot and the human. However, the deformation of the elastic module leads to time-delay perception, which is a threat to the real-time control performance. The time-delay effect is obviously observed in Fig. 9a, which is applied by a PID controller.

To deal with the pure time delay issue of the control system, an alternative solution is the Smith predictor[41]. The Smith predictor is a typical predictive controller concerning pure time delay. Therefore, we also test a PID controller with the Smith predictor as shown in Fig. 9b. Although the time-delay effect has been weakened, the model uncertainties pose a threat to the control system performance, which can be seen at the upper and lower range limits.

Finally, we test our proposed control algorithm as shown in Fig. 9c. The time-delay effect is eliminated as the unstructured uncertainties by the predictive force controller and DoB, along with the model uncertainties. In order to give a distinct comparison, the tracking error corresponding to the three control schemes is presented in Fig. 11. The control performance has been improved,

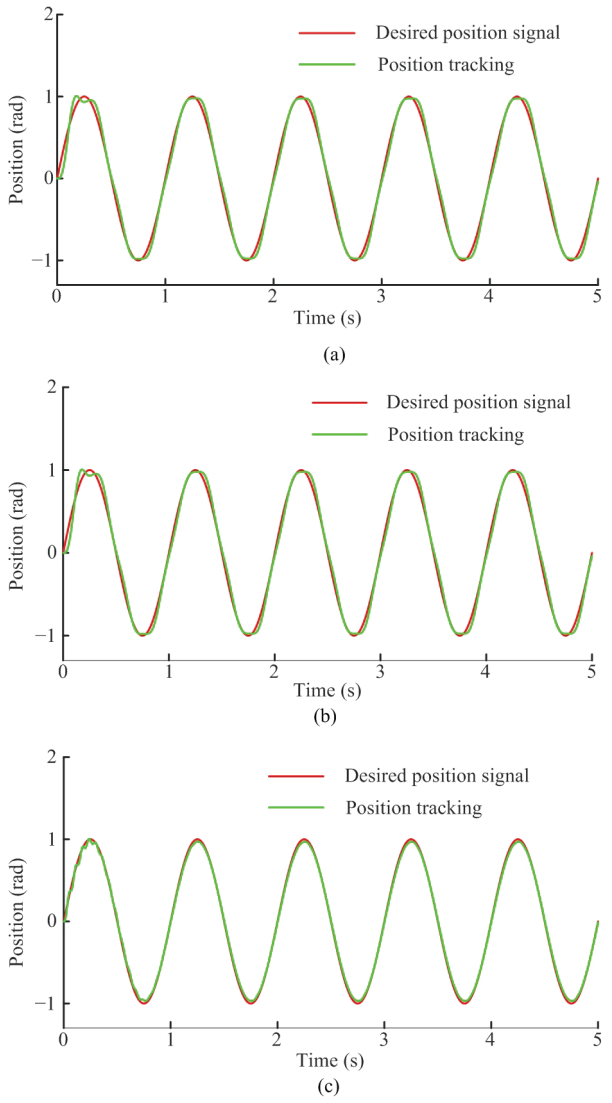

Fig. 9 Comparison of three control schemes. To evaluate our proposed control algorithm, the three different control schemes are compared as shown above.

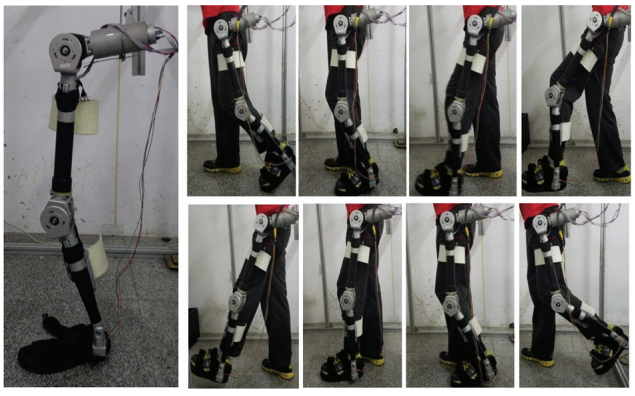

Fig. 10 (a) Singe lower extremity exoskeleton platform; (b) pilot locomotion experiment.

compared with the other two control methods in terms of the time-delay effect as well as the model uncertainties.

The second experiment is conducted to verify the control performance with the human factors as shown in Fig. 11b. During the experiment, the pilot's leg is compliantly attached with the exoskeleton. The exoskeleton is driven by human physical intention, which means that the input signal is obtained from the deformation of the elastic module. The pilot has been asked to test the swing-phase movement in the experiment.

The experimental results have shown that the exoskeleton can track the human motion intention with a slight difference in both hip joint and knee joint, as shown in Figs. 12a and 12b. For further analysis, the information of the desired torque and the generated torque are present in Figs. 13a and 13b. Note that, the generated torque has the component of high-frequency noise and model uncertainties. In addition, compared to the desired torque, the Root Mean Square (RMS) value of the torque error is 4.5%. While for the same situation in the knee joint, the RMS value is 5.5%.

Additionally, compared with the other algorithms, the Root Mean Square Error (RMSE) of the torque error of knee joint is 9%[20], as given in Table 3, which is also tested with single-leg exoskeleton system with series elastic actuators and the algorithm is also based on the compensation of the human interaction which is considered as the disturbance of the control system.

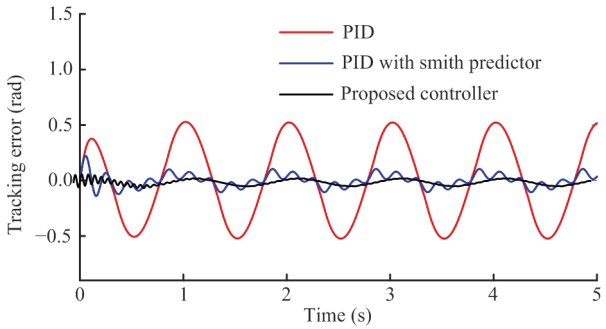

Fig. 11 Tracking errors of three different control schemes, i.e., PID, PID with Smith predictor and proposed control methodology.

Table 3 Properties of the elastic module

Methods	Force control[24]	Force control[20]	Our algorithm
Hip	Not mentioned	Not mentioned	4.5%
Knee	5.5%	9%	5.5%

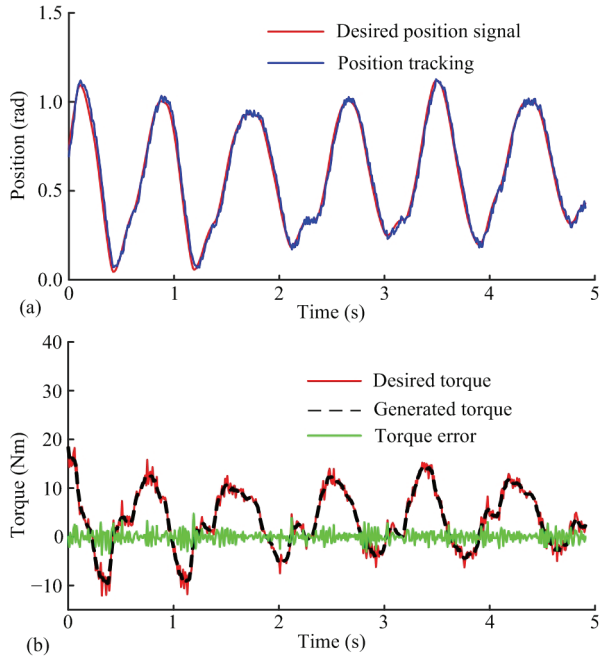

Fig. 12 Experimental results of hip joint while walking. (a) Position tracking of the hip joint; (b) desired torque tracking of the hip joint and corresponding tracking error.

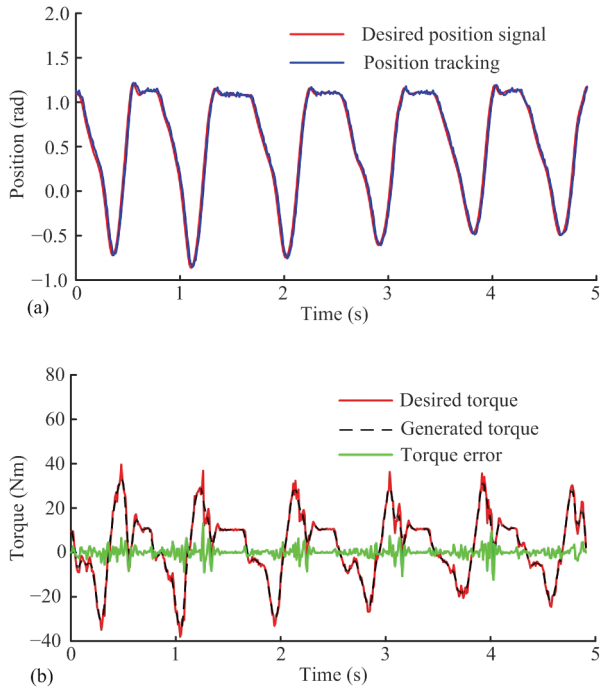

Fig. 13 Experimental results of knee joint while walking. (a) Position tracking of the knee joint; (b) desired torque tracking of the knee joint and corresponding tracking error.

According to the RMS results, our control scheme can provide more precise driven torque and may be more suitable for an exoskeleton application.

The force control[24] is also implemented on the same experiment platform, which can be seen as the improvement of the control scheme[18]. Compared with our control algorithm, although the torque RMS of the knee joint is the same (5.5%), the control platform is only tested with knee joint. Moreover, the control scheme is also addressed in continuous domain, which is not straightforward.

5 Conclusion

In the application related to human augmentation device, the exoskeleton is a kind of robot driven by human intention. However, the precision of the physical HMI recognition is still a strong barrier to improve the control performance. In addition, the time-delay issue may pose a threat to the stability of the control system.

Thus, in this paper, a novel elastic module is designed and its control scheme is proposed. The control algorithm has focused on two aspects, i.e., precision control and robustness enhancement.

The robustness of the control system is guaranteed by the internal model control properties and designed Q filter. In addition, the precision of the control performance is carefully considered from the DoB and feedback loop. The unstructured uncertainties are compensated by the DoB, along with the HMI. The high-frequency noise is eliminated by the Q filter. The feedback loop also takes precaution for the tracking error and seeks for the optimal control inputs. The control performance is verified by the experimental results.

In terms of the real-time control performance, the time-delay issue does not affect the control system. Since the control scheme proposed in this paper is independent of the human physical properties, the designed controller can be used for each individual. Therefore, the proposed control algorithm may provide a feasible solution for the HMI applications.

Acknowledgement

Part of this work was supported by the National Science Foundation of China under Grant No. 51521003.

References

[1] Kazerooni H. Exoskeletons for human power augmentation. *IEEE/RSJ International Conference on Intelligent Robots*

and Systems, *Edmonton*, Alta, Canada, 2005, 3459–3464.

[2] Wang L, Du Z, Dong W, Shen Y, Zhao G. Intrinsic sensing and evolving internal model control of compact elastic module for a lower extremity exoskeleton. *Sensors*, 2018, **18**, E909.

[3] Wang L, Du Z, Dong W, Shen Y, Zhao G. Probabilistic sensitivity amplification control for lower extremity exoskeleton. *Applied Sciences*, 2018, **8**, 525.

[4] Schabowsky C N, Godfrey S B, Holley R J, Lum P S. Development and pilot testing of HEXORR: Hand EXOskeleton rehabilitation robot. *Journal of Neuroengineering and Rehabilitation*, 2010, **7**, 36.

[5] Esquenazi A, Talaty M, Packel A, Saulino M. The ReWalk powered exoskeleton to restore ambulatory function to individuals with thoracic-level motor-complete spinal cord injury. *American Journal of Physical Medicine & Rehabilitation*, 2012, **91**, 911–921.

[6] Kolakowsky-Hayner S A, Crew J, Moran S, Shah A. Safety and feasibility of using the Ekso™ bionic exoskeleton to aid ambulation after spinal cord injury. *The Spine Journal*, 2016, **4**, 003.

[7] Bouzit M, Burdea G, Popescu G, Boian R. The Rutgers Master II-new design force-feedback glove. *IEEE/ASME Transactions on Mechatronics*, 2002, **7**, 256–263.

[8] Nikolakis G, Tzovaras D, Moustakidis S, Strintzis M G. Cybergrasp and phantom integration: Enhanced haptic access for visually impaired users. 9*th Conference Speech and Computer*, Saint-Petersburg, Russia, 2004, **9**, 20–22.

[9] Cruciger O, Schildhauer T A, Meindl R C, Tegenthoff M, Schwenkreis P, Citak M, Aach M. Impact of locomotion training with a neurologic controlled hybrid assistive limb (HAL) exoskeleton on neuropathic pain and health related quality of life (HRQoL) in chronic SCI: A case study. *Disability and Rehabilitation*: *Assistive Technology*, 2016, **11**, 529–534.

[10] Kiguchi K, Hayashi Y. An EMG-based control for an upper-limb power-assist exoskeleton robot. *IEEE Transactions on Systems*, *Man*, *and Cybernetics*, *Part B* (*Cybernetics*), 2012, **42**, 1064–1071.

[11] Wang S, Wang L, Meijneke C, Van Asseldonk E, Hoellinger T, Cheron G, Tamburella F. Design and control of the MINDWALKER exoskeleton. *IEEE Transactions on Neural Systems and Rehabilitation Engineering*, 2015, **23**, 277–286.

[12] Jimenez-Fabian R, Verlinden O. Review of control algorithms for robotic ankle systems in lower-limb orthoses, prostheses, and exoskeletons. *Medical Engineering and Physics*, 2012, **34**, 397–408.

[13] Bouteraa Y, Abdallah I B. Exoskeleton robots for upper-limb rehabilitation. 13*th International Multi-Conference on Systems*, *Signals & Devices* (*SSD*), Leipzig, Germany, 2016, 1–6.

[14] Unluhisarcikli O, Pietrusinski M, Weinberg B, Bonato P, Mavroidis C. Design and control of a robotic lower extremity exoskeleton for gait rehabilitation. *IEEE/RSJ International Conference on Intelligent Robots and Systems* (*IROS*), San Francisco, CA, USA, 2011, 4893–4898.

[15] Tsukahara A, Hasegawa Y, Sankai Y. Gait support for complete spinal cord injury patient by synchronized leg-swing with HAL. *IEEE/RSJ International Conference on Intelligent Robots and Systems* (*IROS*), San Francisco, CA, USA, 2011, 1737–1742.

[16] Carignan C R, Cleary K R. Closed-loop force control for haptic simulation of virtual environments. *Haptics-e*, 2000, **1**, 1–4.

[17] Bae J, Kong K, Tomizuka M. Gait phase-based control for a rotary series elastic actuator assisting the knee joint. *Journal of Medical Devices*, 2011, **5**, 031010.

[18] Bae J, Tomizuka M. A gait rehabilitation strategy inspired by an iterative learning algorithm. *Mechatronics*, 2012, **22**, 213–221.

[19] Vallery H, Ekkelenkamp R, Van Der Kooij H, Buss M. Passive and accurate torque control of series elastic actuators. *IEEE/RSJ International Conference on Intelligent Robots and Systems*, San Diego, CA, USA, 2007, 3534–3538.

[20] Kong K, Bae J, Tomizuka M. Control of rotary series elastic actuator for ideal force-mode actuation in human-robot interaction applications. *IEEE/ASME Transactions on Mechatronics*, 2009, **14**, 105–118.

[21] Kim S, Bae J. Force-mode control of rotary series elastic actuators in a lower extremity exoskeleton using model-inverse time delay control (MiTDC). *IEEE/RSJ International Conference on Intelligent Robots and Systems* (*IROS*), Daejeon, South Korea, 2016, 3836–3841.

[22] Zhang L, Xu D, Makhsous M, Lin F. Stiffness and viscous damping of the human leg. *Proceedings of the* 24*th Annual Meeting of the American Society of Biomechanics*, Chicago, IL. USA, 2000.

[23] Zoss A, Kazerooni H, Chu A. On the mechanical design of the Berkeley lower extremity exoskeleton. *IEEE/RJS International Conference on Intelligent Robots and Systems*, Edmunton, Canada, 2005.

[24] Kong K, Bae J, Tomizuka M. A compact rotary series elastic actuator for human assistive systems. *IEEE/ASME Transactions on Mechatronics*, 2012, **17**, 288–297.

[25] Long Y, Du Z, Cong L, Wang W, Zhang Z, Dong W. Active disturbance rejection control based human gait tracking for lower extremity rehabilitation exoskeleton. *ISA Transactions*, 2017, **67**, 389–397.

[26] Thomson W, Dahleh M. *Theory of Vibration with Applications*, CRC Press, Boca Raton, USA, 1996.

[27] Granata K P, Wilson S E, Padua D A. Gender differences in active musculoskeletal stiffness. Part I.: Quantification in controlled measurements of knee joint dynamics. *Journal of Electromyography and Kinesiology*, 2002, **12**, 119–126.

[28] Granata K P, Padua D A, Wilson S E. Gender differences in active musculoskeletal stiffness. Part II. Quantification of leg stiffness during functional hopping tasks. *Journal of Electromyography and Kinesiology*, 2002, **12**, 127–135.

[29] Singh R M, Chatterji S. Trends and challenges in EMG based control scheme of exoskeleton robots – A review. *International Journal of Scientific & Engineering Research*, 2012, **3**, 933–940.

[30] Khokhar Z O, Xiao Z G, Menon C. Surface EMG pattern recognition for real-time control of a wrist exoskeleton. *BioMedical Engineering Online*, 2010, **9**, 41.

[31] Strausser K A, Kazerooni H. The development and testing of a human machine interface for a mobile medical exoskeleton. *IEEE/RSJ International Conference on Intelligent Robots and Systems* (*IROS*), San Francisco, USA, 2011, 4911–4916.

[32] Garcia C E, Morari M. Internal model control. 1. A unifying review and some new results. *Industrial & Engineering Chemistry Process Design and Development*, 1982, **21**, 308–323.

[33] Economou C G, Morari M, Palsson B O. Internal model control: Extension to nonlinear system. *Industrial & Engineering Chemistry Process Design and Development*, 1986, **25**, 403–411.

[34] Camacho E F, Bordons Alba C. *Model Predictive Control*, Springer-Verlag London Limited, London, UK, 2013.

[35] Cutler C R, Ramaker B L. Dynamic matrix control? A computer control algorithm. *IEEE Transactions on Automatic Control*, 1980, **17**, 72.

[36] Chen W H. Disturbance observer based control for nonlinear systems. *IEEE/ASME Transactions on Mechatronics*, 2004, **9**, 706–710.

[37] Chen W H, Ballance D J, Gawthrop P J, O'Reilly J. A nonlinear disturbance observer for robotic manipulators. *IEEE Transactions on Industrial Electronics*, 2000, **47**, 932–938.

[38] Doyle J C, Francis B A, Tannenbaum A R. *Feedback Control Theory*, Macmillan Publishing Company, London, UK, 1990.

[39] Winter D A. *Biomechanics and Motor Control of Human Movement*, John Wiley & Sons, New York, USA, 2009.

[40] Xi Y G. *Model Predictive Control*. National Defense Industry Press, Beijing, 1993.

[41] Warwick K, Rees D. *Industrial Digital Control Systems*, Institution of Engineering and Technology, London, UK, 1988.

[42] Garcia C E, Prett D M, Morari M. Model predictive control: Theory and practice – A survey. *Automatica*, 1989, **25**, 335–348.

[43] Hou Z S, Xu J X. On data-driven control theory: The state of the art and perspective. *Acta Automatica Sinica*, 2009, **35**, 650 – 667.